Optics Letters

Power-over-fiber in a 10 km long multicore fiber link within a 5G fronthaul scenario

J. D. López-Cardona,[1] S. Rommel,[2] E. Grivas,[3] D. S. Montero,[1] M. Dubov,[4] D. Kritharidis,[5] I. Tafur-Monroy,[2] and C. Vázquez[1,*]

[1]Electronics Technology Dpt., Universidad Carlos III de Madrid, Avda. de la Universidad 30, 28911, Leganés (Madrid), Spain
[2]Institute for Photonic Integration, Eindhoven University of Technology, Eindhoven, The Netherlands
[3]Eulambia Advanced Technologies, Agia Paraskevi, Athens, Greece
[4]Optoscribe Ltd., Rosebank Technology Park, Livingston, UK
[5]Intracom Telecom, Markopoulou Avenue, Peania, Athens, Greece
*Corresponding author: cvazquez@ing.uc3m.es

Received 29 July 2021; revised 1 October 2021; accepted 1 October 2021; posted 6 October 2021 (Doc. ID 439105); published 21 October 2021

We evaluate the impact of Power-over-Fiber (PoF) technology on the fronthaul of a 5G-NR network with an Analog-Radio-over-Fiber at 25.5 GHz on a 10 km long multicore fiber. The study in this Letter analyzes the bit error rate (BER) performance for different levels of energy transmitted by the PoF system. 133 mW of maximum optical power at reception is demonstrated showing negligible BER impact or data transmission BER improvement in a dedicated and shared scenario.

https://doi.org/10.1364/OL.439105

Power-over-Fiber (PoF) technology is a good strategy for providing energy to remote points free of electromagnetic interference, with low-weight, good galvanic isolation and with an easy integration within the telecommunication operators infrastructure. Optical fibers are also among the technologies supporting the increasing capacity of 5G radio access networks (RAN), as part of the back/fronthaul infrastructure for transmitting radio-over-fiber (RoF) signals.

The new 5G-NR technology paradigm with centralized architecture (CRAN) reduces resource requirements and simplifies network management and maintenance by reducing the complexity of the remote radio heads (RRHs). These new features mean a significant reduction in RRH power consumption. This optimization makes it possible to use PoF technology to feed some critical elements, with the corresponding advantage of a centralized remote control and power supply—all from the optical domain. Some studies show that it is possible to achieve a reduction in consumption of up to 40% [1]. In this sense, it is proposed to implement sleep modes in the RRH based on an intelligent control of the resources according to the traffic and the number of users [2]. Others proposed switching the energy between different RRHs, depending on traffic demand [3] through a software defined network. A summary about the main achievements in PoF applied to RoF for different types of fibers and commercial products is reported in [4]. This includes the use of multicore fibers (MCFs) as in [5–7] for driving an analog photoreceiver in the 90 to 110 GHz band at short distances in a dedicated scenario; that is, data are sent in a different core to the one used for energy delivery. On the other hand, a 20 m 4-MCF link is used for optically powering in [8], in both a dedicated and shared scenario with data and energy in the same core. The use of the MCF in optical fronthauling [9,10] is currently under development to increase the capacity of the infrastructure while providing compact deployments. On the other hand, PoF technology and 5G technology with different modulation schemes are reported in [11], and the need of new strategies for efficiently powering 6G networks, including PoF capability, is currently pointed out [12].

In this Letter, we evaluate the PoF technology in the fronthaul scenario of a 5G-NR network from a base band unit (BBU) providing data traffic with quadrature phase-shift keying (QPSK) modulation and 800 MHz of bandwidth, in a 10 km long MCF as part of an Analog-Radio-over-Fiber (ARoF) link. The evaluation is carried out by analyzing the bit error rate (BER) behavior for different power transmission levels. Additionally, some relevant BBU and MCF parameters for the study are characterized.

In the following, the experimental setup is described. The proposed system is developed in the framework of the blueSPACE project (EU H2020 5G-PPP) [10], and it is composed of two systems: the baseband unit (ARoF BBU) and the power transmitter (PoF system). For this experiment, the BBU is configured to generate a QPSK modulation with 800 MHz of bandwidth. Two configurations are used—with and without a radio link of 9 m in the 3GPP n258 band. The experiment uses a 10 km long link of a seven-core MCF fiber. A local oscillator ($F_{LO} = 10.25$ GHz) is injected into the first Mach–Zehnder (MZM_1), configured in an optical carrier suppression mode. The second Mach–Zehnder (MZM_2) is used to modulate the electrical signal at an intermediate frequency (IF_{TX}) of 5 GHz. Core number 7 is used to send the ARoF signal; meanwhile, the core number 4 sends a copy of the two-tone signal after MZM_1, which is used on the remote site to perform the downconversion. The millimeter-wave RF signal is generated by

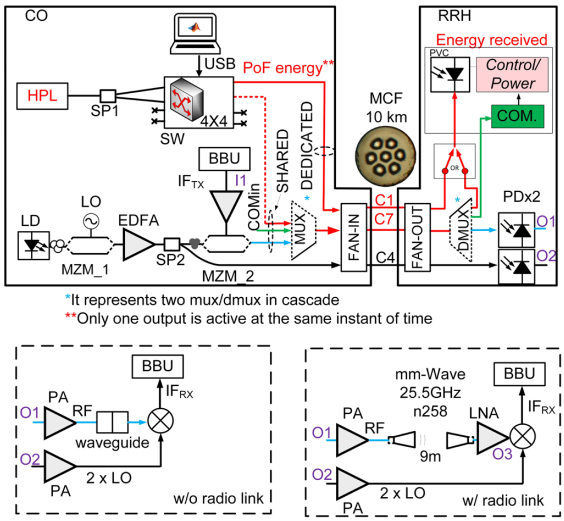

Fig. 1. Integration of a PoF and ARoF in a 5G-NR scenario, with and without the radio links included.

Table 1. Analysis of BER Stability at BBU

Attenuation (dB)	Average	STD
0	<1 E-9	<1 E-9
10	8.97 E-8	1.41 E-8
14	1.87 E-5	1.96 E-6

optical heterodyning of the modulated two-tone signal on the photodetector (PD) at the RRH, resulting in an RF carrier (F_{RF}) of 25.5 GHz, given by the expression $F_{RF} = IF_{TX} + 2 \cdot F_{LO}$. The remaining elements are used for amplification and conditioning of the ARoF signal. For more details; see [13]. The PoF system consists of a high-power laser (HPL) at a 1480 nm wavelength, an optical splitter (SP1, 50:50), an optical switch (4 × 4), and the photovoltaic cells (PVCs). This PVC has a maximum optical power of 200 mW and operates in the range between 1300 and 1600 nm. The control of the switching is done externally via a USB interface, which allows us to select the type of scenario: shared or dedicated. In the shared scenario, data and power are multiplexed through core number 7 while, in the dedicated scenario, power is sent only through core number 1; see Fig. 1.

In order to validate the integration of 5G-NR and PoF technology, the time-dependent behavior of the BER in the two PoF scenarios and for the two configurations is analyzed. The objectives of this characterization are (1) to evaluate the BER stability in a back-to-back configuration (B2B, IF_{TX} connected to IF_{RX}), (2) to measure the transfer function and estimate the fiber chromatic dispersion, and (3) to calculate the PoF transmission system efficiency at 1480 nm.

The BBU stability analysis is performed at different attenuation levels of the IF_{TX} output signal: 0, 10, and 14 dB. These levels replace the insertion losses introduced by the ARoF system. Table 1 shows the average BER and standard deviation (STD) for the different attenuation values. The BER values, as expected, increase as the power of the intermediate frequency signal decreases, with the standard deviation always being lower than the average value.

The measurement of the transfer function of the MCF allows estimating the BER behavior due to the combined impact of chromatic dispersion and self- and cross-phase modulation (SPM and XPM) nonlinear effects, both of significant relevance in PoF and RoF systems, depending on power levels and link lengths. The fiber-induced SPM improves the frequency-length product by shifting the power fading to higher frequencies [14], in comparison to power fading provoked only by chromatic dispersion [15]. In [11], a simulation performed using a Virtual Photonics Instrumentation Tool, shows the impact of both effects (SPM and XPM) on a 10 km SMF ARoF link at 17 GHz with PoF in a shared scenario. It is observed that, at low HPL power levels (<800 mW), the impact of both effects is negligible. In our experiments, we are working with power levels within the MCF below 500 mW, so these effects are not going to be significant. The measurement of the transfer function of the MCF helps us to confirm that the transmitted RF signal is far away from the critical frequency affected by power fading. On the other hand, both phenomena are sensitive to power instabilities, and the HPL can induce noise in the data channel through stimulated Raman scattering (SRS) [16]. The Brillouin effect has not been considered, since the linewidth of the HPL laser used is larger than 2 nm [4]. In the experiment, the transmission parameter S21 is determined using the spectrum analyzer N9918A, which is configured as a network analyzer. Figure 2 shows a simplified schematic of the measurement setup in which MZM_1, LO, EDFA, and SP2 have been omitted, and the LO oscillator is disabled. This is done by injecting the excitation of the analyzer through the MZM_2 driver (point I1; see Fig. 2) and measuring the response at the PD output (point O1; see Fig. 2).

Initial calibration is performed by removing only the MCF in order to eliminate the effect of the other elements of the system on the measurement. Once the calibration procedure is completed, the S21 parameter is measured. Figure 3 shows the measurement and theoretical estimation of the fiber transfer function. Additionally, it is observed that the critical frequency value is approximately 18.20 GHz, and hence the chromatic dispersion is 18.85 ps/nm/km [15], matching previous measurements. The system energy efficiency (SEE) has been calculated in both scenarios—shared (SEE_{shared}) and dedicated ($SEE_{dedicated}$) [17].

This parameter is the ratio between the maximum electrical power delivered by the PVC and the HPL optical emitted power. The optical power received at the remote site is +18.96 (78.70 mW) and +21.23 dBm (132.74 mW) for the shared and dedicated scenarios, respectively, when the HPL laser is configured with an emission power of +31 dBm (1.26 W). This maximum power is intended to assure that no more than 500 mW are injected into the MCF. Additionally, open circuit voltage (V_{oc}) and short circuit current (I_{sc}) have been measured for different HPL power levels (P_{HPL}) and PVC input powers (P_{PVC}); see Table 2. Considering a 30% optical-to-electrical efficiency of the PVCs, the SEE_{shared} and $SEE_{dedicated}$ are approximately 1.80% and 3.10%, respectively.

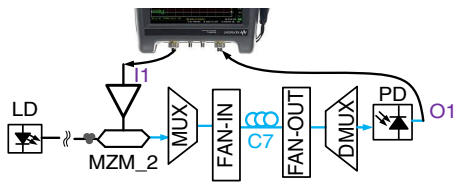

Fig. 2. Measurement of the transfer function of the MCF.

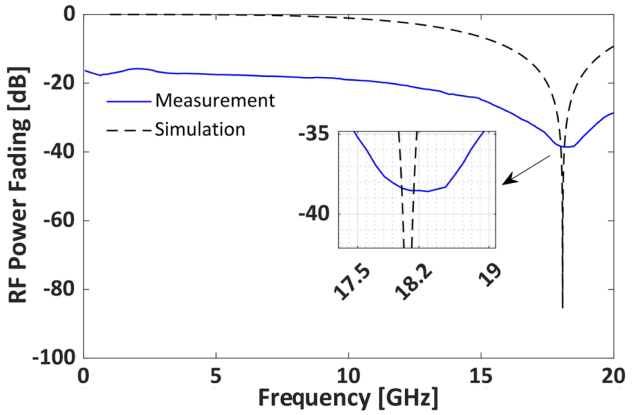

Fig. 3. Theoretical and measured transfer function of the MCF (core 7).

Table 2. PVC Short-Circuit Current and Open Circuit Voltage for Different HPL Power Levels

P_{HPL} [dBm]	P_{PVC} [dBm]	I_{sc} [mA]	V_{oc} [V]
DEDICATED SCENARIO			
29	19.19	10.14	3.95
30	20.21	13.04	3.97
31	21.23	15.98	3.99
SHARED SCENARIO			
29	16.98	6.24	3.87
30	17.96	7.95	3.91
31	18.96	9.87	3.96

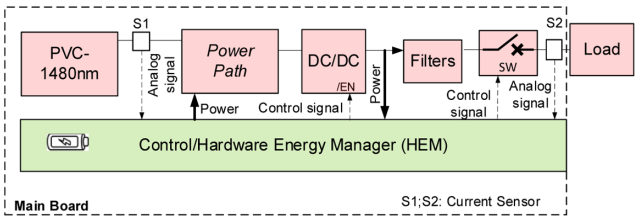

Fig. 4. Schematic of different building blocks of a MB, including a PVC connection.

The PVC is connected to a main board (MB) controlled by a MSP430F5636 microcontroller. The MB has a built-in auxiliary communication channel; see COM in Fig. 1, which allows commands to be received from the central office (CO). This channel allows us to control and synchronize the MB functionalities such as a low consumption mode (see [2]) from the CO. The MB includes different devices for power management: power path, filters, and a DC/DC converter with the capability of tracking the maximum power point of the PVC to operate at the optimal point; see Fig. 4.

On the other hand, the impact of power transmission in the shared (core 7) and dedicated (core 1) scenarios has been evaluated with and without a radio link. The analysis is carried out for 72 s with a sampling rate of 3 s. thus guaranteeing a reliable BER measurement. The HPL laser is set to: OFF and from +27 to +31 dBm in 1 dB steps. Figure 5 shows the main results of the experiment without a radio link included. The BER value

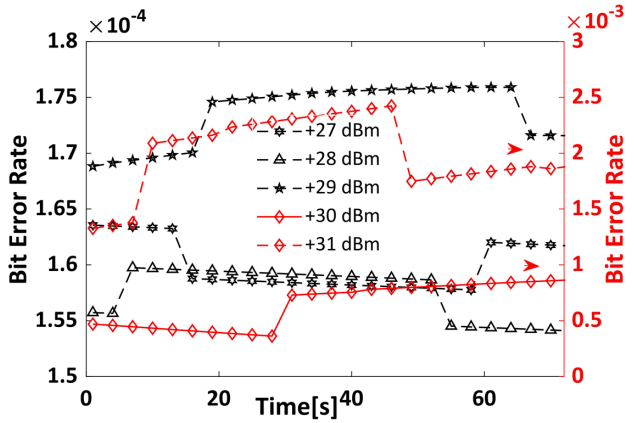

Fig. 5. BER performance in the shared scenario without a radio link.

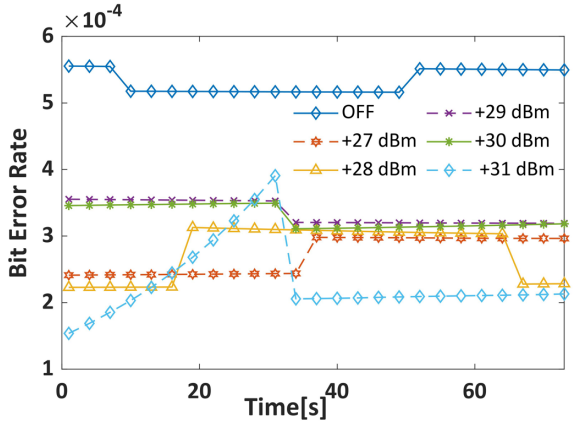

Fig. 6. BER performance in the shared scenario with a radio link.

obtained at OFF state is 1.89 E-4, which is used as a reference to compare with the rest of the HPL optical powers.

In all cases, the BER performance is slightly higher as the laser power increases, reaching a maximum average value of 2.00 E-3. In the dedicated scenario, the BER value remains invariant with respect to the HPL power emission condition at OFF state. The intercore MCF crosstalk (IC-XT) measured is lower than −50 dB, and there is a narrow-band demultiplexer at the reception stage with −24 dB crosstalk. In terms of IC-XT fluctuations, they are minimized as the HPL is a broadband source with 2 nm linewidth [18]. In the shared scenario, power fluctuations can affect the transmission quality, along with the BBU instabilities. We measure the temporal response of the HPL in the electrical domain and observe the maximum noise value to be around 30 dBm. The HPL noise is transferred to a data channel through SRS after a 10 km link length provoking small BER variations for different power levels, as shown in Fig. 5, being greater for 30 and 31 dBm.

Increasing the MCF core density will straightforward increase the overall delivered PoF power at the remote site. However, IC-XT decreases exponentially with core-to-core separation [19], and its impact on the data traffic quality and resulting BER performance should be carefully analyzed.

The study with a radio link is performed by including in the previous system two horn antennas separated by 9 m. The BER performance is evaluated for the same power levels as the

previous experiment. Figure 6 shows the results obtained for the shared scenario and, in all cases, the performance is worse, except for the HPL levels with higher noise.

In this Letter, we have demonstrated the feasibility of integrating PoF technology in the fronthaul of a 5G network with and without a wireless radio link. The experimental results have shown that the impact of power transmission in some cases improves the BER value, a result of interest for data transmission. The maximum transmitted optical power (133 mW) can be increased by optimizing the insertion loss of the system elements or using MCF designs that allow higher injected powers. To the best of our knowledge, there are no previous results of delivering PoF in a 10 km 7-MCF in coexistence with an ARoF transmission as a fronthaul of a high-bandwidth wireless link in the 3GPP n258 band.

Funding. Comunidad de Madrid (Y2018/EMT-4892); Ministerio de Ciencia, Innovación y Universidades (RTI2018-094669-B-C32); Horizon 2020 Framework Programme (762055).

Acknowledgment. The support of Juliana Barros and Dimitrios Konstantinou is acknowledged.

Disclosures. The authors declare no conflicts of interest.

Data Availability. Data underlying the results presented in this Letter are not publicly available at this time but may be obtained from the authors upon reasonable request.

REFERENCES

1. Z. Tan, C. Yang, and Z. Wang, J. Lightwave Technol. **35**, 2669 (2017).
2. J. D. López-Cardona, R. Altuna, D. S. Montero, and C. Vázquez, J. Lightwave Technol. **39**, 4951 (2021).
3. G. O. Pérez, J. D. López-Cardona, R. Muñoz, C. Vázquez, D. Larrabeiti, R. Vilalta, J. A. Hernández, and J. M. Fàbrega, in *European Conference on Optical Communication (ECOC)* (2018).
4. C. Vázquez, J. D. López-Cardona, P. Lallana, D. S. Montero, F. M. A. Al-Zubaidi, S. Pérez-Prieto, and I. P. Garcilópez, IEEE Access **7**, 158409 (2019).
5. T. Umezawa, A. Kanno, K. Akahane, Y. Awaji, and N. Yamamoto, in *42nd European Conference on Optical Communication (ECOC)* (2016), p. 3.
6. T. Umezawa, K. Kashima, A. Kanno, A. Matsumoto, K. Akahane, N. Yamamoto, and T. Kawanishi, IEEE J. Sel. Top. Quantum Electron. **23**, 23 (2017).
7. T. Umezawa, P. T. Dat, K. Kashima, A. Kanno, N. Yamamoto, and T. Kawanishi, J. Lightwave Technol. **36**, 617 (2018).
8. C. Vázquez, D. S. Montero, F. M. A. Al-Zubaidi, and J. D. López-Cardona, in *European Conference on Networks and Communications (EuCNC)* (2019).
9. W. Kong, Y. Sun, C. Cai, and Y. Ji, in *Conference on Lasers and Electro-Optics* (2020), paper JTu2A.25.
10. S. Rommel, D. Pérez-Galacho, J. M. Fabrega, R. Muñoz, S. Sales, and I. Tafur Monroy, IEEE Trans. Broadcast. **65**, 434 (2019).
11. F. M. A. Al-Zubaidi, J. D. López-Cardona, D. S. Montero, and C. Vázquez, J. Lightwave Technol. **39**, 4262 (2021).
12. N. Chen and M. Okada, IEEE Internet Things J. **8**, 8719 (2020).
13. S. Rommel, D. Dodane, E. Grivas, B. Cimoli, J. Bourderionnet, G. Feugnet, Á. Morales, E. Pikasis, C. Roeloffzen, P. V. van Dijk, M. Katsikis, K. Ntontin, D. Kritharidis, I. Spaleniak, P. Mitchell, M. Dubov, J. B. Carvalho, and I. T. Monroy, J. Lightwave Technol. **38**, 5412 (2020).
14. F. Ramos, J. Marti, V. Polo, and J. M. Fuster, IEEE Photonics Technol. Lett. **10**, 1473 (1998).
15. U. Gliese, S. Norskov, and T. N. Nielsen, IEEE Trans. Microw. Theory Tech. **44**, 1716 (1996).
16. C. Headley and G. P. Agrawal, *Raman Amplification in Fiber Optical Communication Systems* (Elsevier/Academic, 2005).
17. C. Vázquez, D. S. Montero, P. J. Pinzón, J. D. López-Cardona, P. Contreras, and A. Tapetado, Proc. SPIE **10128**, 101280E (2017).
18. B. J. Puttnam, G. Rademacher, and R. S. Luís, Optica **8**, 1186 (2021).
19. K. Saitoh and S. Matsuo, J. Lightwave Technol. **34**, 55 (2016).